Journal of Chromatography A 1756 (2025) 466095

Contents lists available at ScienceDirect

Journal of Chromatography A

journal homepage: www.elsevier.com/locate/chroma

Hydrophobic interaction chromatography (HIC) isotherm incorporating salt-dependent water activity enhances model-based analysis of protein elution profiles

Ronald Jäpel [a], Matthias Knödler [b], Eric von Lieres [a,c], Johannes Felix Buyel [d,*]

[a] Forschungszentrum Jülich, IBG-1: Biotechnology, 52428 Jülich, Germany
[b] RWTH Aachen University, Institute of Molecular Biotechnology, 52074 Aachen, Germany
[c] RWTH Aachen University, Computational Systems Biotechnology, 52074 Aachen, Germany
[d] BOKU University, Department of Biotechnology and Food Sciences (DBL), Institute of Bioprocess Science and Engineering (IBSE), Muthgasse 18, 1190 Vienna, Austria

ARTICLE INFO

Keywords:
CADET
Linear gradient
Mechanistic model
Protein binding
Separation prediction

ABSTRACT

Hydrophobic interaction chromatography (HIC) is a highly relevant separation technique that provides orthogonal selectivity to widely used ion exchange chromatography (IEC). However, in contrast to the latter, the mechanisms underlying hydrophobic interaction are difficult to capture in the form of an isotherm, probably due to the complex nature of the mechanisms involved. Of the several HIC isotherms that have been proposed, one improved the prediction accuracy by accounting for the water molecules released upon protein binding which was estimated based on the concentration of protein bound to the stationary phase. However, we found that this isotherm resulted in implausible predictions depending on the selected chromatographic conditions. For example, when altering the protein concentration of salt gradient elution experiments the location of the elution peak shifted drastically. Upon investigating the assumptions made during isotherm development, we replaced the previous estimate with a salt concentration-dependent water activity (SWA). Accordingly, our SWA isotherm utilizes the activity of the surrounding water molecules to describe the activity of the released bulk-like water molecules. We evaluated this new isotherm on *in silico* and experimental datasets and found that the unrealistic predictions disappeared. Additionally, the precision of elution profile prediction, measured as the differences in elution peak height, skew and position, improved by an average of 2.8-fold and up to 5.6-fold. We also augmented the isotherm into a unified form that can account for pH effects as well. Lastly, we implemented the isotherms in CADET, so they can easily be used from within the software suite.

1. Introduction

Hydrophobic interaction chromatography (HIC) is a workhorse in many bioprocesses including biopharmaceutical manufacturing. For example, >99.5 % purity can be achieved with >95 % recovery in case of antibody purification [1]. Like with other types of chromatography, a plethora of parameters can be modified during HIC in order to achieve optimal process results, typically high product recovery and purity [2]. These parameters include, amongst others, the ligand type, salt and buffer type as well as the corresponding concentrations, pH, temperature and flow rate. Accordingly, optimizing HIC steps is labor, time and cost intensive, even if small scale and high-throughput technologies are used.

One option to streamline and de-bottleneck HIC process development is the use of predictive models, which facilitate *a priori* predictions about potentially useful parameter combinations and thereby guide and limit experimental efforts [3]. The models can be data-driven, hybrid or mechanistic. Mechanistic models, like the general rate model (GRM) of chromatography, facilitate reliable predictions about chromatographic separation [3] and typically include descriptions for convective mass transfer, diffusion and solute-ligand interactions [4]. The latter are often formulated as sorption isotherms, which provide a quantitative description of the equilibrium between the adsorbed and free amounts of a solute [5].

Whereas simple isotherms consider only an equilibrium constant (e.g. Freundlich isotherm) and maximum binding capacity of the stationary

* Corresponding author.
E-mail addresses: r.jaepel@fz-juelich.de (R. Jäpel), matthias.knoedler@rwth-aachen.de (M. Knödler), e.von.lieres@fz-juelich.de (E. von Lieres), johannes.buyel@rwth-aachen.de (J.F. Buyel).

https://doi.org/10.1016/j.chroma.2025.466095
Received 4 March 2025; Received in revised form 23 May 2025; Accepted 24 May 2025
Available online 25 May 2025

phase (e.g. Langmuir isotherm), more complex isotherms have been developed that account for process parameters as well as the specifics of the proposed binding mechanisms. For example, in HIC, protein binding to stationary phase ligands is assumed to result in the release of previously bound water molecules into the mobile phase and the number of water molecules is assumed to increase with increasing salt concentration in the mobile phase [6,7] (see Section 3). Accordingly, isotherms accounting for the salt concentration and its effect on the binding equilibrium have been developed [6,7]. A more recent isotherm accounting for the effects of water on hydrophobic surfaces (WHS isotherm) appeared to achieve particularly good agreements between experimental data and model predictions [8].

However, when using this isotherm in our simulations, we found implausible predictions such as an increase in protein binding at decreasing salt concentration (see 4.1). We therefore investigated the assumptions made during isotherm formulation and identified the root cause. We then re-formulated the isotherm assuming that the water molecules released upon protein binding are indistinguishable from other water molecules in the mobile phase. We used a salt-dependent water activity (SWA) isotherm and found that the new isotherm substantially outperformed the original WHS isotherm when applied on both synthetic *in silico* and experimental data of albumin and lysozyme. We also compared the SWA isotherm with previous isotherms and found that it provided superior performance in most cases. Finally, we augmented and unified the HIC isotherms to account for potential pH effects as well, which allows it to be used in a flexible manner, for example from within the CADET simulation suit [9] into which it is now integrated.

2. Material and methods

2.1. Data sources for osmotic coefficients and densities for HIC isotherms

The influence of the sodium chloride concentration on the density of an aqueous solution of sodium chloride at 298.15 K was taken from literature [10] and interpolated using a second-degree polynomial function ($R^2 = 1.0000$). The osmotic coefficients for sodium chloride solutions at 298.15 K were taken from literature [11] ($n = 17$) and interpolated using a fifth degree polynomial function ($R^2 = 1.0000$, predicted $R^2 = 0.9884$). The osmotic coefficients for sodium phosphate solutions at 298.15 K were taken from literature [12] and interpolated using a linear function ($R^2 = 0.9999$).

2.2. Chromatographic experiments

All buffers for modeling experiments (Supplementary Table 1) were prepared using ultrapure water with a conductivity <5.5 µS m^{-1} to diminish fluctuations of the ionic strength. Ultrapure water was purified using an Arium-pro UV ultra-pure water system (Sartorius, Göttingen, Germany). All buffers used for the modeling experiments were clarified by 0.2 µm filtration using a Nalgene Rapid-Flow vacuum bottle top filter (Thermo Fisher Scientific, Waltham, USA) and a N816 vacuum pump (KNF Neuberger, Freiburg, Germany).

Model protein candidates (Table 1) were bought at Sigma Aldrich (St. Louis, USA) and dissolved at a concentration of 3.0 mg mL^{-1} in HIC binding buffer (Supplementary Table 1). Prior to injection, the protein solutions were filtered through 0.2 µm MiniSart syringe sterile filters (Sartorius, Göttingen, Germany). For gradient elution the Äkta pure 25 L chromatography system (Cytiva, Little Chalfont, UK) equipped with a 1 mL OPUS MiniChrom chromatography column (Table 2) (Repligen, Waltham, USA) was used at a constant flow rate of $1.6 \bullet 10^{-4}$ m s^{-1} (0.5 mL min^{-1}).

Gradient elution experiments were conducted for each specific protein for pH values of 6.0, 7.0, and 8.0 with gradient lengths of 5, 10, 15, 30, 45, 60 and 120 CV at a constant flow rate of $1.6 \bullet \times 10^{-4}$ m s^{-1} (0.5 ml min^{-1}). The columns were equilibrated for 5 CV in elution buffer followed by 10 CV high salt binding buffer (Supplementary Table 1). A 1 mL capillary loop was mounted onto the injection valve and manually filled with the 1 mL protein solution with a concentration of 3 mg mL^{-1} using a 2 mL needle-less syringe (B. Braun, Melsungen, Germany). After injection of 100 µL protein solution, the column was washed for 10 CV with binding buffer and the elution gradient with low salt elution buffer was started (Supplementary Table 1). Conductivity, UV280nm and pH signals were recorded and exported as ASCII files using the Unicorn v. 6.4 Evaluation software (Cytiva, Little Chalfont, UK).

These experiments were performed at pH 6.0, 7.0, and 8.0 each for Lysozyme on the Butyl Sepharose resin, for Lysozyme on the Phenyl Sepharose resin and for bovine serum albumin on the Butyl-S Sepharose resin.

All salt gradients were also performed once with a zero dead volume connector (Cytiva, Little Chalfont, UK) in place of the column.

2.3. Simulation in CADET for batch adsorption data

A model with a single unit operation was set up in CADET-Core v4.4.0 to simulate the batch adsorption experiments (Table 3). The unit operation was modeled using the lumped rate model without pores (i.e. an intraparticle porosity of 0) with an interparticle porosity of 0.5, a length of 0.1 m and a cross-sectional area of 0.01 m^2. It was discretized using only a single axial cell. At 0 s, the column was set to contain a given concentration of salt and proteins solved in the liquid phase and no protein bound to the stationary phase. Simulations were run until equilibrium was reached, which was defined as a <0.01 % change in concentrations over the last two seconds in the mobile and stationary phase.

Binding model parameters for Fig. 2A were chosen as follows: K_{eq}, n, and q_{max} for all four isotherms were chosen freely to optimize readability of the graphs. Specifically, the parameters were selected so that in a non-saturated state of the stationary phase the binding equilibrium resulted in an equal distribution of bound and free state of a hypothetical protein (i.e. 50 % of the protein mass bound to the stationary phase, 50 % in solution). Please note that such a condition was impossible to achieve for the WHS isotherm due to its ever-changing equilibrium state. Additionally, the parameters were chosen so that saturation effects set in at around 10^{-5} mol l^{-1} and full saturation (overloaded by a factor of 100) at around 10^{-3} mol l^{-1}. For the WHS isotherm β_0 and β_1 were taken from [8]. The remaining parameters for the other three isotherms (β_0 and β_1 for the SWA isotherm, β_0, K_s, ϵ, and ρ for the Deitcher isotherm, and K_p and K_s for the Mollerup isotherm), were adjusted so that the isotherm predictions best matched the WHS predictions. The effect of parameter scales was assessed for all isotherms using the parameters listed in

Table 1
Model proteins. Information about the purity, molecular mass and pI were given by the manufacturer.

Protein	Manufacturer	Purity [%]	m_M [kDa]	pI [-]
Bovine serum albumin (monomer)	Sigma Aldrich	≥ 97	66.5	4.7
Lysozyme	Sigma Aldrich	≥ 98	14.3	11.3

Table 2
HIC resins used for chromatography modelling. Information about the ligand structure, particle size and pore radius were taken from literature [13].

Resin name	Ligand	Manufacturer	Particle size [µm]	Pore radius [nm]
Phenyl Sepharose 6 FF HS	Phenyl	Cytiva	~90	~27
Butyl Sepharose 4 FF	Butyl	Cytiva	~90	~27
Butyl-S Sepharose 4 FF	Butyl-S	Cytiva	~90	~27

Table 3
Parameters for the simulation of batch adsorption data in CADET (Fig. 2A).

Parameter	WHS	Deitcher	Mollerup	SWA
q_{max} [mol m_{SP}^{-3}]	$4.0 \bullet 10^{-4}$	$5.5 \bullet 10^{-4}$	$5.4 \bullet 10^{-4}$	$4.5 \bullet 10^{-4}$
K_{eq} [m_{MP}^3 m_{SP}^{-3}]	0.3	0.95	0.29	0.85
n [-]	3	9.02	10	9.02
c_s [mol m^{-3}]	120	120	120	120
β_0 [-]	0.03	2	n.a.	2
β_1 [m_{MP}^3 mol^{-1}]	1.001	n.a.	n.a.	0.57
K_s [m_{MP}^3 mol^{-1}]	n.a.	0	0.01	n.a.
K_p [m_{MP}^3 mol^{-1}]	n.a.	n.a.	0	n.a.
ϵ [m_{SP}^3 mol^{-1}]	n.a.	0	n.a.	n.a.
ρ [m_{MP}^3 mol^{-1}]	n.a.	$3.4 \bullet 10^{-2}$	n.a.	$3.4 \bullet 10^{-2}$

Table 4
Settings used to assess the impact of parameter scale on predictions made with different isotherms. In addition to the values listed (mol m^{-3} or mmol l^{-1}), the parameters were re-scaled to mol l^{-1} and μmol l^{-1} to assess the impact on corresponding simulation results (Fig. 2B–D).

Parameter	WHS	Deitcher	Mollerup	SWA
q_{max} [mol m_{SP}^{-3}]	$1.0 \bullet 10^4$	$1.0 \bullet 10^4$	$1.0 \bullet 10^4$	$1.0 \bullet 10^4$
K_{eq} [m_{MP}^3 m_{SP}^{-3}]	1.0	1.0	1.1	1.1
n [-]	0.1	2.0	1.0	2.0
c protein [mol m_{MP}^{-3}]	5.0	5.0	5.0	5.0
β_0 [-]	0.03	0.5	n.a.	2
β_1 [m_{MP}^3 mol^{-1}]	3	n.a.	n.a.	0.57
K_s [m_{MP}^3 mol^{-1}]	n.a.	$1.4 \bullet 10^{-4}$	$1.5 \bullet 10^{-4}$	n.a.
K_p [m_{MP}^3 mol^{-1}]	n.a.	n.a.	0	n.a.
ϵ [m_{SP}^3 mol^{-1}]	n.a.	0	n.a.	n.a.
ρ [m_{MP}^3 mol^{-1}]	n.a.	0.0335	n.a.	0.0335

Table 4.

2.4. CADET-based simulation of chromatograms

Chromatograms were simulated in CADET-Core v4.4.0 using CADET-Process v0.9.1. The system was set up with an inlet, a column unit operation and an outlet. The concentration profile for the inlet was taken from the zero dead volume gradient experiment (see Section 2.2). The inlet unit operation was connected directly to the column unit operation. The column was set up with the lumped rate model with pores (Table 5). The column was connected directly to the outlet, at which the concentration profile was recorded.

2.5. Isotherm parameter estimation based on linear gradient elution experiments

CADET-Process was used with the U_NSGA3 genetic algorithm to determine all binding parameters on sets of three linear gradient elution experiments (5 cv, 30 cv and 120 cv). The optimizer hyperparameters were left at the default values. The optimization objective was set to the *shape* difference metric as defined by CADET-Process with the options *use_derivative* set to *false* and *include_height* set to *true*.

Table 5
Parameters used for the lumped rate model with pores transport model.

Parameter	Value
Axial dispersion [m_{MP}^2 s^{-1}]	$4.5 \bullet 10^{-7}$
Column length [m]	$2.0 \bullet 10^{-2}$
Column porosity (i.e. inter-particle) [-]	0.18
Film diffusion [m_{MP} s^{-1}]	$9.6 \bullet 10^{-7}$
Particle porosity (i.e. intra-particle) [-]	0.59
Particle radius [m]	$4.5 \bullet 10^{-5}$
Column diameter [m]	$8.0 \bullet 10^{-3}$

2.6. Estimation of parameters based on batch adsorption data

Parameters were fitted using a sum of squared differences gradient descent with the least_squares function from scipy.optimize. The addition of one percent of noise was calculated by multiplying the dataset values with random numbers equally distributed between 0.99 and 1.01.

For fitting that included only the parameters k_{eq} and q_{max}, the remaining parameters required for batch adsorption simulations (β_0, β_1, and n) were obtained as follows: For the WHS isotherm, values were taken from [8]. For the SWA isotherm, values were generated by fitting the full isotherm to simulated batch adsorption data generated using the full WHS parameter set from [8] and then disregarding the parameters k_{eq} and q_{max} for subsequent fitting runs.

3. Theory and calculation

3.1. Binding stoichiometry calculation

The adsorption process during HIC can be modeled as the stoichiometric interaction between the protein molecules P in solution and a number n of unoccupied ligands L which upon protein binding form protein-ligand complexes PL_n (Eq. (1)) [6].

$$P + nL \leftrightarrow PL_n \tag{1}$$

Building on previous reports [7,14], a recent study suggests to consider the water molecules W in this equation [8], because they stabilize the hydrophobic surfaces of both dissolved proteins and ligands before the interaction by forming well-ordered structures (Eq. (2)) [15–17].

$$P + nL \leftrightarrow PL_n + n\beta W \tag{2}$$

Upon protein-ligand binding, a number of β water molecules is released from each of the n ligands L involved in the binding of one protein. The released water molecules are thought to adopt an unordered state as do the water molecules in the rest of the bulk mobile phase, which is the entropic driving force of protein-ligand interaction in HIC. Using a previously proposed method [18], Eq. (2) can be converted into Eq. (3) to facilitate a calculation of the equilibrium distribution K.

$$K = \frac{a_{PL_n} \cdot a_W^{n\beta}}{a_P \cdot a_L^n} \tag{3}$$

Here, a is the chemical activity of the component indicated by the respective subscript (here: L – ligand; P – protein; W – water). Because the activities cannot be measured directly, they need to be approximated based on the component concentrations in the system.

3.2. Using compound activities

The mobile phase protein activity a_p can be approximated from the protein concentration in this phase, c_p, using a fitted modulation parameter K_p, the salt concentration c_s, and a fitted modulation parameter K_s (Eq. (4)) [6].

$$a_P = c_P \cdot e^{K_p c_p + K_s c_s} \tag{4}$$

The adsorbed protein activity a_{PLn} can be approximated from the bound protein concentration q. In the literature, the adsorbed protein activity is assumed to be independent of the salt concentration in the mobile phase [7]. However, lateral interactions between adsorbed proteins can be accounted for using an empirical relationship that incorporates a fitted loading dependence parameter ϵ (Eq. (5)).

$$a_{PL_n} = q \cdot (1 + \varepsilon \cdot q) \tag{5}$$

Similarly, an expression for the activity of water molecules involved in

the binding process $a_w{}^{n\beta}$ has to be defined. These can range from a simple linear model with a fitted linear coefficient ρ (Eq. (6)) [7] to complex models ((Eq. (7) and Eq. (22)).

$$a_W^{n\beta} = (e^{\rho c_s})^{n\beta} \tag{6}$$

In contrast to Eq. (6), some authors assumed that the water activity is directly correlated with the stationary phase protein concentration q, with each protein releasing ν water molecules upon ligand binding and ν being independent of the salt and protein concentrations (Eq. (7)) [8].

$$a_W^{n\beta} \cong \nu q^{n\beta} \tag{7}$$

These authors used a formula (Eq. (8)), which is usually applied to calculate the hydration number of salt ions [19], to estimate the number of water molecules β released per ligand L, as these two processes were assumed to be equivalent [8].

$$\beta = \beta_0 e^{\beta_1 c_s} \tag{8}$$

Where β_0 is the stoichiometric number of water molecules released in the absence of salt and β_1 is a salt concentration-dependent factor scaling the number of release water molecules.

3.3. Available ligands calculation

At this point, the last remaining unknown in the equilibrium constant equation (Eq. (3)) is the activity of free ligands a_L^n, which will be approximated with the concentration of free ligands, c_L^n. This parameter can be calculated based on the total capacity Λ, the number of hydrophobic binding sites n and a steric hindrance factor s using Eq. (9) [8].

$$c_L^n = (\Lambda - (n+s)q)^n \tag{9}$$

Because the total capacity Λ is difficult to determine experimentally, it can be approximated by the saturation capacity (Eq. (10)), which is protein-specific.

$$q_{max} = \frac{\Lambda}{n+s} \tag{10}$$

Inserting Eq. (9) into Eq. (10) yields Eq. (11) to estimate the concentration of free ligands. While this equation still includes Λ, it allows us to later isolate the effects from Λ from concentration dependent effects in Eq. (13).

$$c_L^n = \left(1 - \frac{q}{q_{max}}\right)^n \cdot \frac{1}{\Lambda^n} \tag{11}$$

3.4. Definition of the equilibrium constant

Inserting all parametrizations (Equations4, 5, 6 and 11) into Eq. (3) gives Eq. (12) as an alternative parametrization of the equilibrium distribution.

$$K = \frac{q(1+\epsilon \cdot q)(e^{\rho c_s})^{n\beta}}{c_P \cdot e^{K_p c_p + K_s c_s} \cdot (1 - q/q_{max})^n \cdot 1/\Lambda^n} \tag{12}$$

Collecting all factors which do not involve protein or salt concentrations on the left-hand side yields Eq. (13) specifying the equilibrium constant k_{eq}.

$$k_{eq} = K\Lambda^n = \frac{q(1+\epsilon \cdot q)(e^{\rho c_s})^{n\beta}}{c_P \cdot e^{K_p c_p + K_s c_s} \cdot (1 - q/q_{max})^n} \tag{13}$$

Assuming that the protein-ligand interaction is close to the thermodynamic equilibrium but time-dependent, Eq. (14) is used for the kinetic formulation of the adsorption isotherm [8].

$$k_{kin}\frac{dq}{dt} = k_{eq}\left(1 - \frac{q}{q_{max}}\right)^n c_p \; e^{K_p c_p} \; e^{K_s c_s} - q(1+\epsilon q)(e^{\rho c_s})^{n\beta} \tag{14}$$

Here k_{kin} is the kinetic constant. Replacing k_{kin} with k_d^{-1} and k_{eq} with $k_a k_d^{-1}$ gives an equivalent formulation (Eq. (15)), which is more in line with the conventions used in the CADET software [9,20].

$$\frac{dq}{dt} = k_a\left(1 - \frac{q}{q_{max}}\right)^n c_p \; e^{K_p c_p} \; e^{K_s c_s} - k_d q(1+\epsilon q)(e^{\rho c_s})^{n\beta} \tag{15}$$

Reduced versions of this equation have been used in the literature, such as in Eq. (16) [6], which does not include the influence of released water molecules. Eq. (16) will be referred to as the Mollerup isotherm in this study.

$$\frac{dq}{dt} = k_a\left(1 - \frac{q}{q_{max}}\right)^n c_p \; e^{K_p c_p} \; e^{K_s c_s} - k_d q \tag{16}$$

Similarly, Eq. (17) [7] does not account for the influence of liquid-phase protein concentration on the respective activity, and will be referred to as the Deitcher isotherm in this study.

$$\frac{dq}{dt} = k_a\left(1 - \frac{q}{q_{max}}\right)^n c_p \; e^{K_s c_s} - k_d q(1+\epsilon q)(e^{\rho c_s})^{n\beta} \tag{17}$$

3.5. Alternative definition of water activity

Including the alternative approximation for the activity of water molecules from Eqs. (7) and (8) in Equation 15while removing the fitted parameters K_p, K_s, ϵ, and ρ, gives Eq. (18) [8].

$$\frac{dq}{dt} = k_a\left(1 - \frac{q}{q_{max}}\right)^n c_p - k_d \cdot q \cdot \nu \cdot q^{n\beta} \tag{18}$$

As the effect of the stochiometric factor ν is not distinguishable from the effect of k_d, these two terms are combined into k_d' which yields Eq. (19). This equation is referred to as the water-on-hydrophobic-surfaces (WHS) isotherm from hereon, based on the title of the original publication.

$$\frac{dq}{dt} = k_a\left(1 - \frac{q}{q_{max}}\right)^n c_p - k_d' \cdot q \cdot q^{n\beta} \tag{19}$$

4. Results and discussion

4.1. Unexpected results using a water-on-hydrophobic-surfaces (WHS) isotherm

Using the WHS isotherm to simulate HIC produced unexpected results. First, one would expect that at a constant salt concentration and in a non-saturated state (i.e., $q << q_{max}$), the equilibrium between bound protein and non-bound protein should not be affected by the absolute protein concentration. Specifically, when neglecting saturation effects, proteins in both low and highly concentrated samples should exhibit the same strength of interaction with the resin and should elute at the same time during gradient elution experiments.

However, when using the WHS isotherm, low concentration protein samples resulted in stronger interaction with a resin (later elution) compared to a high concentration setting. The reason for this was that in the isotherm (Eq. (19)) the bound and free protein concentrations are raised to different exponents (i.e. 1 for c_p and $1 + n\beta$ for q). As both n and β are always positive, the exponent of q is always larger than the exponent of c_p.

The second unmet expectation was that an increasing the salt concentration would permit more protein to bind to the resin. When using the WHS isotherm at protein concentrations greater than 1.0 – regardless of the concentration units, the effect of the salt concentration was reversed.

This behavior arises because dq/dt decreases as the concentration of bound protein q increases. In simple terms, the more protein is bound, the slower the additional binding becomes. The influence of q on dq/dt is

expected to be diminished for high salt concentrations, allowing for more protein to bind. For the WHS, this desirable behavior only holds when the concentration of q is below the numerical value 1.0. While this is the case, an increase in salt concentration c_s increases the value of β and reduces the term $q^{n\beta}$ towards zero, thereby minimizing the influence of q on dq/dt. However, if q rises above 1.0, increasing c_s amplifies the effect of q on dq/dt. Therefore, if the bound protein concentration exceeds 1.0, an increase in the salt concentration causes a decrease in the bound protein concentration. Because the CADET framework expresses concentration in mol m^{-3} of stationary phase, the threshold value of 1.0 is frequently exceeded. For example, lysozyme loaded onto Phenyl Sepharose 6 FF at pH 6.0 exhibited a dynamic binding capacity of 3.6 mol m^{-3} [21] (Supplementary Table 2).

This also causes the WHS isotherm's predictions to change with the choice of unit system, an outcome that is physically inconsistent and therefore unexpected. When the calculation units are changed from mol l^{-1} to µmol l^{-1}, the numerical value of q is rescaled, potentially shifting it from below to above the critical threshold of 1.0. This shift reverses the direction of the influence of salt on the binding equilibrium.

Both issues can be resolved if yet another definition of water activity a_w is used that does not depend on the protein concentration (Eq. (20)).

$$k_{kin}\frac{dq}{dt} = k_{eq}\left(1 - \frac{q}{q_{max}}\right)^{n} c_p - q \cdot a_w^{n\beta} \tag{20}$$

4.2. Alternative salt-dependent water activity (SWA) isotherm

Here, we modeled the water activity as a linear function of the salt concentration, creating a salt-dependent water activity (SWA) isotherm. We expanded on the relationship described in Eq. (6) with Eq. (21):

$$\ln(a_W) = -\sum_i m_i \cdot \Phi_i \cdot M_W \tag{21}$$

Where m_i is the molality of salt ions in mol kg^{-1} of water, Φ_i is the osmotic coefficient of the salt ions and M_w is the molar mass of water [22]. Due to the low concentration of the phosphate buffer of 25 mmol l^{-1} it reduces the water activity only by 0.002 based on data previously published data [12]. This is only a difference of 2.1 % compared to the difference in water activity caused by the sodium chloride included in the same buffer and was therefore considered to be negligible. Additionally, extending CADET to include multiple salt species would have exceeded the scope of this study and hard coding a fixed buffer system into an isotherm would be bad practice, because any future change in the buffer system would require the modification of CADET source-code and a recompilation of CADET. Therefore, we decided to limit the water activity calculations to sodium chloride (Eq. (22)).

$$a_w = e^{-c_s \cdot 2 \cdot \Phi_{NaCl} M_W} \tag{22}$$

Here c_s is the sodium chloride concentration, Φ_{NaCl} is the combined osmotic coefficient of sodium chloride (as defined in Section 2.1), and the factor 2 is due to the sum over both sodium and chloride ions. This leads to the isotherm shown in Eq. (23), which we refer to as the salt-dependent water activity (SWA) HIC model.

$$k_{kin}\frac{dq}{dt} = k_{eq}\left(1 - \frac{q}{q_{max}}\right)^{n} c_p - q \cdot \left(e^{-c_s \cdot 2 \cdot \Phi_{NaCl} M_W}\right)^{n\beta_0 \exp(\beta_1 c_s)} \tag{23}$$

Two simplifying assumptions were made here. The first is that a constant osmotic coefficient for sodium chloride was used instead of a concentration dependent one [11]. The discrepancy between the two calculations can be compensated by multiplying β_0 by 0.95 and β_1 by

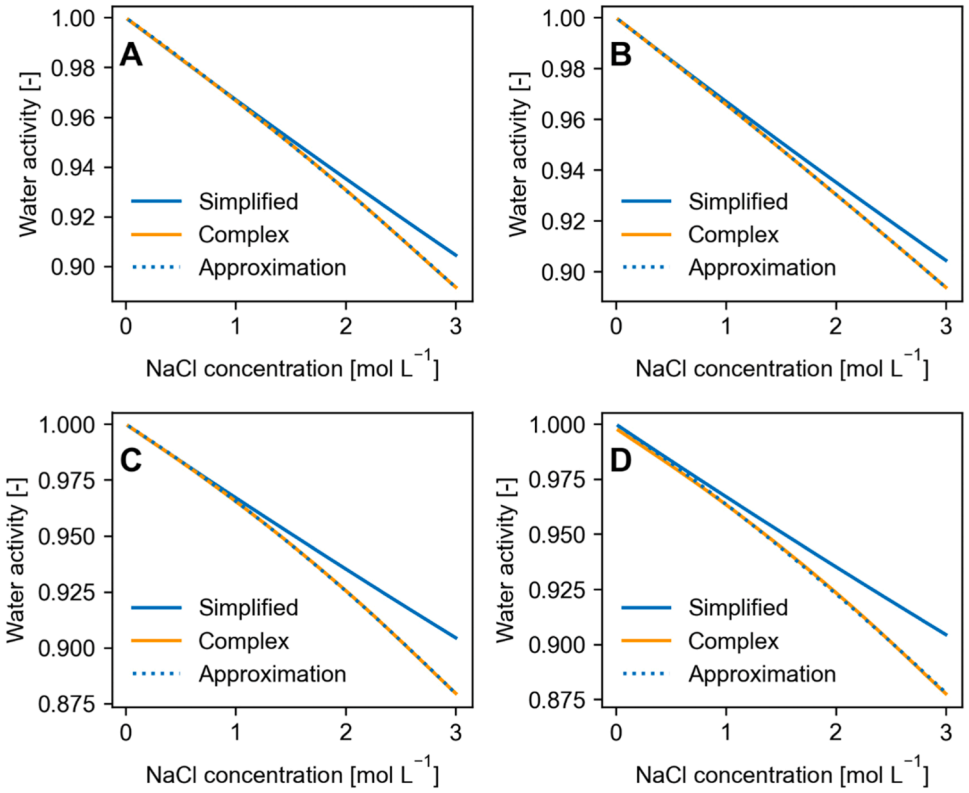

Fig. 1. Assessment of reliability of water activity calculation. Water activities were calculated for different sodium chloride concentrations using a simplified approach (blue) implemented for the SWA isotherm (Eq. (22)) and compared to a set of more complex alternatives (orange) as well as approximations of the complex curves using the simplified results with offsets in β_0 and β_1 (dotted blue). A. A concentration-dependent osmotic coefficient was used for the complex calculation. B. A molality instead of a molarity was used for the complex model. C. The complex used molality and concentration-dependent osmotic coefficients. D. The complex model used molality, concentration-dependent osmotic coefficients and included the influence of phosphate buffer.

0.062 (SSE of $3.5 \bullet 10^{-7}$; Fig. 1A). The compensation was calculated by minimizing the sum of squared errors between the complex model and the approximated model predictions for the water activity from 0.0 to 3.0 mol l^{-1} while changing the multiplicative factors for β_0 and β_1 using the scipy.optimize.least_squares function [23].

The second assumption is that the calculations were done using the molarity of sodium chloride instead of the molality, because the CADET framework calculates only molarities. Implementing the correct conversion from molarity to molality into the CADET framework was beyond the scope of this study and would most likely not have improved the prediction quality, because the discrepancy can be compensated by multiplying β_1 with 0.0372 (Fig. 1B) (SSE $5.68 \bullet 10^{-9}$). The combined effect of the first and second simplification can also be compensated by multiplying β_0 by 0.95 and β_1 by 0.099 (SSE $3.27 \bullet 10^{-7}$; Fig. 1C). Only if the influence of the phosphate buffer is added to the extended model, then changes in β_0 and β_1 cannot entirely compensate the differences resulting in a sum of squared errors of $1.13 \bullet 10^{-5}$ between the complex model and an approximation using the SWA isotherm (Fig. 1D).

As per the definition of an isotherm, the model does not include the effect of temperature on protein-ligand interactions. The model can be extended to include such temperature effects in the future, but we expect the impact to moderate because in the temperature range of 15–25 °C the osmotic coefficient and the density coefficients reported in literature varied <1.5 % [10–12]. For the simplified SWA isotherm, this temperature-caused offset in Φ_{NaCl} could be entirely offset by dividing β_0 by the value of the offset.

4.3. A unified isotherm for hydrophobic interaction chromatography

Next, we derived a unified HIC isotherm (UNI) by combining the SWA isotherm with all additional terms in two previous publications [6, 7] isotherms (Eqs. (24) and 25).

$$\frac{dq}{dt} = k_a \left(1 - \frac{q}{q_{max}}\right)^n c_p \, e^{K_p c_p} \, e^{K_s c_s} - k_d (1 + \epsilon q) q (e^{\rho c_s})^{n \beta_0 \exp(\beta_1 c_s)} \tag{24}$$

$$\rho = -2 \Phi_{NaCl} M_W \tag{25}$$

The UNI isotherm allows for the easy selection of model subsets by setting specific parameters to zero. For example, if β_1 and K_p are set to zero, the unified HIC isotherm is equivalent to an earlier formulation [7].

A simple multi-component generalization for m binding components is given below (Eqs. (26) and 27).

$$\frac{dq_i}{dt} = k_{a,i} \left(1 - \sum_{j=0}^{m} \frac{q_j}{q_{max,j}}\right)^{n_i} c_{p,i} \, e^{K_{p,i} c_{p,i}} e^{K_s c_s} - k_{d,i} (1 + \epsilon_i q_i) q_i (e^{\rho c_s})^{n_i \beta_0 \exp(\beta_1 c_s)} \tag{26}$$

Building on previous works [24,25], we also suggest the following pH-dependent extension of the unified HIC isotherm:

$$\frac{dq_i}{dt} = k_{a,i} e^{k_{a,lin,i} \cdot pH} \left(1 - \sum_{j=0}^{m} \frac{q_j}{q_{max,j}}\right)^{n_i + n_{lin,i} \cdot pH} c_{p,i} \, e^{K_{p,i} c_{p,i}} e^{K_s c_s} - k_{d,i} (1 + \epsilon_i q_i) q_i (e^{\rho c_s})^{(n_i + n_{lin,i} \cdot pH) \beta_0 \exp(\beta_1 c_s)} \tag{27}$$

4.4. Comparison of isotherm performance

Next, we tested the performance of the different isotherms in terms of simulation of protein adsorption. To do so, all discussed HIC isotherms (WHS, Mollerup, Deitcher, and SWA) were implemented in CADET to simulate synthetic and experimental batch adsorption data as well as linear gradient elution experiments. Importantly, we were able to reproduce the batch adsorption results outside of CADET using independent Python code, which was an additional confirmation that our results are reliable.

4.4.1. In silico batch adsorption calculations

We used synthetic batch adsorption data for an initial performance test. (see 2.3). The fraction of bound to total protein remained about constant in case of the Mollerup, Deitcher, and SWA isotherms in the low protein concentration range until saturation effects started to dominate the interaction (Fig. 2A). In contrast, the WHS isotherm produced an unintuitive, increasing fraction (up to 100 %) of bound protein as the total protein amount decreased (see 4.1).

Likewise, the apparent effect of salt in the system (i.e. stronger binding with increasing salt concentration) was inverted for the WHS isotherm and prediction results were dependent on the scale at which parameters (e.g. salt concentrations) were used (Fig. 2B). The latter is not the case for the Mollerup, Deitcher, and SWA isotherms (i.e. the units chosen for the calculations do not influence the simulation results) (Fig. 2C and D).

In summary, the SWA isotherm (as well as the UNI isotherm) manages to solve the two major problems of the WHS isotherm by having stable equilibrium states at low protein concentrations (Fig. 2A) and by producing identical results regardless of the units used to express concentrations (Fig. 2D), as do the Deitcher and Mollerup isotherms (Fig. 2C).

4.4.2. Fitting to experimental batch adsorption data

After ensuring the theoretical validity of the SWA isotherm, its ability to describe experimental batch adsorption data was investigated based on a previously published dataset [8]. The datapoints in the dataset were manually extracted from Fig. 3 of that publication (Supplementary Fig. 1). Isotherm parameters were estimated from this data as described in Section 2.6.

To investigate the stability of parameter estimates, the dataset was modified with one percent of noise. When estimating all binding parameters with one percent of noise over ten replicates the average coefficient of variance of the estimated parameters was 0.51, with individual parameters reaching coefficients of variance of up to 2.09. Hence, the estimation of all binding parameters based on batch adsorption data was considered to be an ill-conditioned problem as there appear to be redundancies in the isotherm for the application to batch adsorption data.

Parameter estimation was therefore restricted to only include the parameters that [8] originally estimated based on batch adsorption data, namely k_{eq} and q_{max}. This setup resulted in an average coefficient of variance of 0.027, which we considered acceptable.

The sum of squared differences between the WHS-generated batch adsorption data with one percent of noise and the best fit using the SWA isotherms over 20 repetitions was over 48 times lower than the sum of squared differences between the experimental data and the best isotherm fits over 20 repetitions (Fig. 3).

The two isotherms are practically indistinguishable over salt concentrations from 0.0 to 3.0 mol l^{-1} and protein amounts from 10^{-4} to 1.0 mol l^{-1} but diverge for lower protein concentrations. As no further data for the correct behavior at low protein concentrations was available, no quantitative conclusion could be drawn from this disparity.

In conclusion, the SWA isotherm is able to closely approximate batch adsorption data generated by the WHS isotherm, except for very low protein concentrations, and had a 6.3 % lower SSE for fits to experimental data.

4.4.3. In silico chromatographic predictions

Both isotherms were capable of simulating chromatographic protein elution within the CADET framework. On first glance, peak shapes appeared plausible (Supplementary Figs. 2 and 3). An initial, qualitative sensitivity analysis (Fig. 4) confirmed the implausible protein concentration effects when using the WHS isotherm. Specifically, as before (see Fig. 2), the equilibrium state of the WHS isotherm was dependent on the

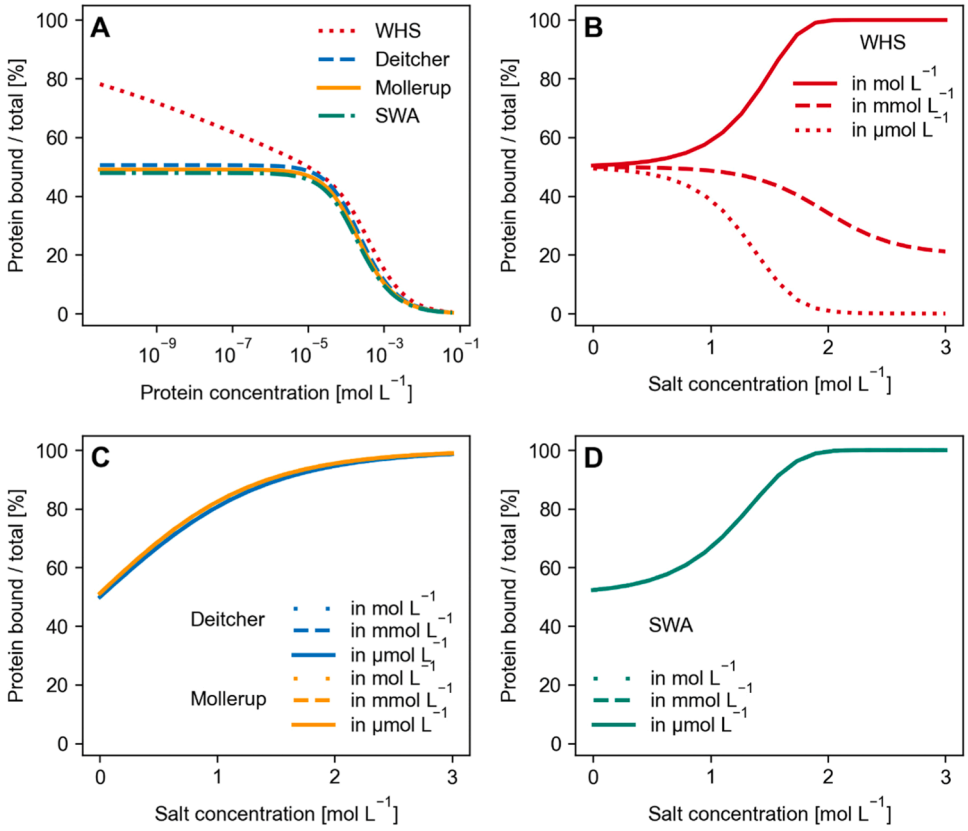

Fig. 2. Simulated batch adsorption data for the water on hydrophobic surfaces (WHS), Deitcher, Mollerup, and salt-dependent water activity (SWA) isotherm (parameter values given in Tables 3 and 4). A. Equilibrium of bound protein vs protein in solution over a range of total protein amounts added to 1.0 L of mobile phase and 1.0 L of stationary phase. B. Batch adsorption using the WHS isotherm over a range of unit systems. C and D. Batch adsorption using the Deitcher and Mollerup, and SWA isotherm respectively over a range of unit systems. The unit system shown in the datapoint label specifies the units used to perform the calculation, while the x-axis specifies the actual salt concentration within the model in mol l^{-1}. For example, at x-axis position 2 mol l^{-1}, the "mol l$^{-1\prime\prime}$ simulation uses "2 mol l$^{-1\prime\prime}$ whereas at the same position the "mmol l$^{-1\prime\prime}$ simulation uses "2000 mmol l^{-1}".

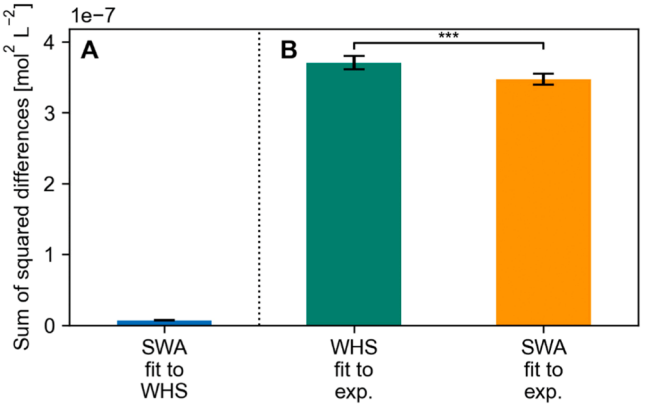

Fig. 3. The sum of squared differences between batch adsorption data and the best fit using the WHS and SWA isotherm ($n = 20$). A: Parameters β_0, β_1, n, k_{eq}, and q_{max} estimated for the SWA isotherm based on simulated batch adsorption data using the WHS isotherm with 1 % added noise. B: Parameters k_{eq} and q_{max} estimated based on experimental data with 1 % added noise. Asterisks indicate significance: $^*p \leq 0.05$, $^{**}p \leq 0.01$, $^{***}p \leq 0.001$.

protein concentration, even below saturation concentrations. This led to a concentration dependent shift in the elution salt concentration. In contrast, the SWA isotherm did not exhibit such artifacts (Fig. 4B).

4.4.4. Experimental chromatography data prediction

We used three sets of gradient elution experiments to assess the performance of the different isotherms. Each set contained a 5 cv, 30 cv and 120 cv linear gradient elution experiments. The objective scores were the differences in the timing, height, and shape of the elution peaks, as defined in the CADET-Process objective function *"Shape"*, using the default parameters from CADET-Process [26] (Fig. 5, Supplementary Fig. 4). The difference in elution peak shape was measured in the objective function by first computing a normalized cross-correlation between experimental and simulated signals that calculates the Pearson correlation coefficient between the signals for each discrete time-increment offset. Then the objective was calculated as 1 minus the maximum Pearson correlation in the cross-correlation. This objective and all subsequent objectives were capped from 0 to +1 by using a sigmoid function transformation, so that 0 is the best result and 1 is the worst result. The temporal offset that produced the maximum Pearson correlation was used as the metric for the time difference, normalized by the absolute length of the experiment and the sigmoid function. The difference in peak height was the absolute difference in height between the peaks, normalized by the height of the target peak and the sigmoid function. Further details on the implementation and default parameters can be found in the documentation of CADET-Process [26].

The WHS isotherm performed significantly worse than all other isotherms on the Lysozyme data sets but significantly better on the albumin dataset (fitted parameters are listed in Supplementary Table 3). The Deitcher and Mollerup isotherms perform identically across all datasets. The SWA and UNI isotherms (the unified isotherm which combines all model parameters from Mollerup, Deitcher and SWA, Eq. (24)) perform better than Deitcher and Mollerup on the Lysozyme on

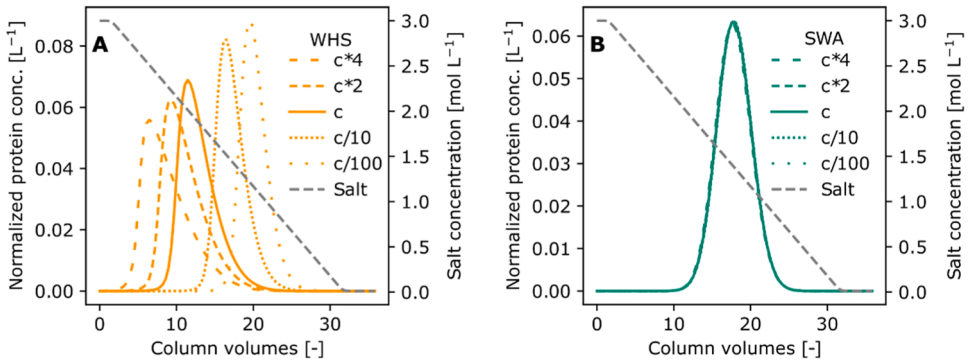

Fig. 4. Simulated 30 cv chromatographic elution using the water on hydrophobic surfaces (WHS; A) and salt-dependent water activity (SWA; B) isotherms for different protein concentrations in the feed. The line "c" illustrates the original protein concentration (c = 0.21 mmol l^{-1}) at which the isotherm parameters were fitted to experimental data (Supplementary Table 3). The left y-axis denotes the normalized protein concentration which was calculated by dividing the protein elution concentration by the area under the protein elution curve.

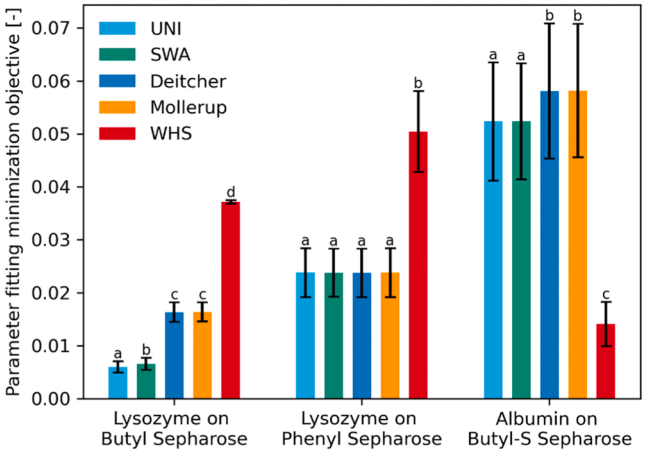

Fig. 5. Parameter fitting objective performance for the isotherms over three protein – column combinations averaged over n = 9 datapoints (3 pH values (6.0, 7.0, and 8.0) times 3 fitting repetitions using random sample with the hopsy function). A lower objective score is better, an objective score of 0.0 would indicate a perfect fit between target and simulation. The input dataset for each fit consisted of a 5 cv, 30 cv and 120 cv gradient elution run. Within each protein – column combination, the letters a, b, c and d mark groups with no significant differences within each group but between each group with a level of p $\leq$ 0.05 based on a paired t-test.

Butyl Sepharose and on the albumin dataset. The UNI isotherm performs slightly but significantly better than the SWA isotherm on the Lysozyme on Butyl Sepharose dataset only.

Regardless of the data, the WHS isotherm produced tailing elution behavior (Figs. 6–8). This was a poor match for the lysozyme dataset but accidentally in a good agreement with the albumin data. The inherent tailing shape of the WHS isotherm is due to the increase in the binding strength as protein concentrations decrease, which is a consequence of the scale-sensitive formulation of the isotherm, as derived in Section 4.1. and simulated in Sections 4.4.1 and 4.4.3 (Figs. 2 and 4). Specifically, the protein concentration decreases during elution increasing the binding strength in case of the WHS isotherm and resulting in a predicted tailing elution. Another consequence of this effect is that the WHS isotherm produces wider elution profiles compared to the SWA isotherm. Because these properties are not linked to protein or column properties but represent an artifact of the WHS isotherm, we regarded the apparently good performance of WHS in combination with albumin a coincidence, which should not be taken into account when attempting to generalize the isotherm performance.

The SWA, Mollerup and Deitcher isotherms struggled to explain the tailing elutions found in the albumin dataset but were capable of simulating the fronting elution observed in the Lysozyme dataset. This is consistent with previously published results for ion exchange chromatography datasets from the same experimental setup where wide, tailing elutions were not reproducible with the lumped rate model with pores together with the SMA binding model [27].

This performance is also in line with the results reported in [6], where the authors compared the performance of the WHS isotherm against the Mollerup and Deitcher isotherms on a single dataset consisting of three glucose oxidase step elutions (Fig. 4 in [6]). These experiments feature strongly tailing elution behaviour, which is favourable for the WHS isotherm due to its inherent tailing shape, as discussed above. The authors fitted the WHS isotherm on an albumin and a lysozyme dataset too, where the WHS isotherm predicted tailing elution behaviour even though this was inconsistent with the experimental elution peaks (Fig. 1d-i in [6]). Unfortunately, the authors did not report the WHS isotherm performance in comparison to that of the Mollerup and Deitcher isotherms for these albumin and lysozyme datasets and a feedback on the performance was pending by the time of the revision of this article.

Therefore, the issue in this HIC example is likely not due to the binding isotherms, but rather to limitations in the transport model or inconsistencies in the experimental data, as previously discussed [27]. Potential contributing factors are hydrodynamic effects such as back mixing, wall effects, and the use of small columns. Future studies could investigate these factors using experiments with varying column sizes and configurations, tests on diffuser and collector influence, and simulations using full GRM and 2D GRM models. Additional research directions include evaluating the effects of impurities, protein multimerization, self-interactions, and potential ion-exchange interactions in HIC. Other possibilities involve studying multiple binding states or orientations through multistate HIC simulations, conducting higher-purity experiments, analysing eluate size distributions via MALS, and re-injecting eluates using fluorescently labelled proteins.

In summary, the SWA isotherm offers significant improvements over the WHS isotherm by removing its instabilities and providing better agreement with experimental data, particularly for narrow, sharp elution peaks. Its ability to simulate tailing elutions warrants further investigation in future studies. Additionally, the SWA isotherm achieves a better fit for two out of the three datasets compared to both the Mollerup and Deitcher isotherms.

5. Conclusions

HIC is a relevant purification method for various biomolecules but the complex interactions underlaying the sorption procedure are difficult to reproduce in mechanistic models. We have expanded previous

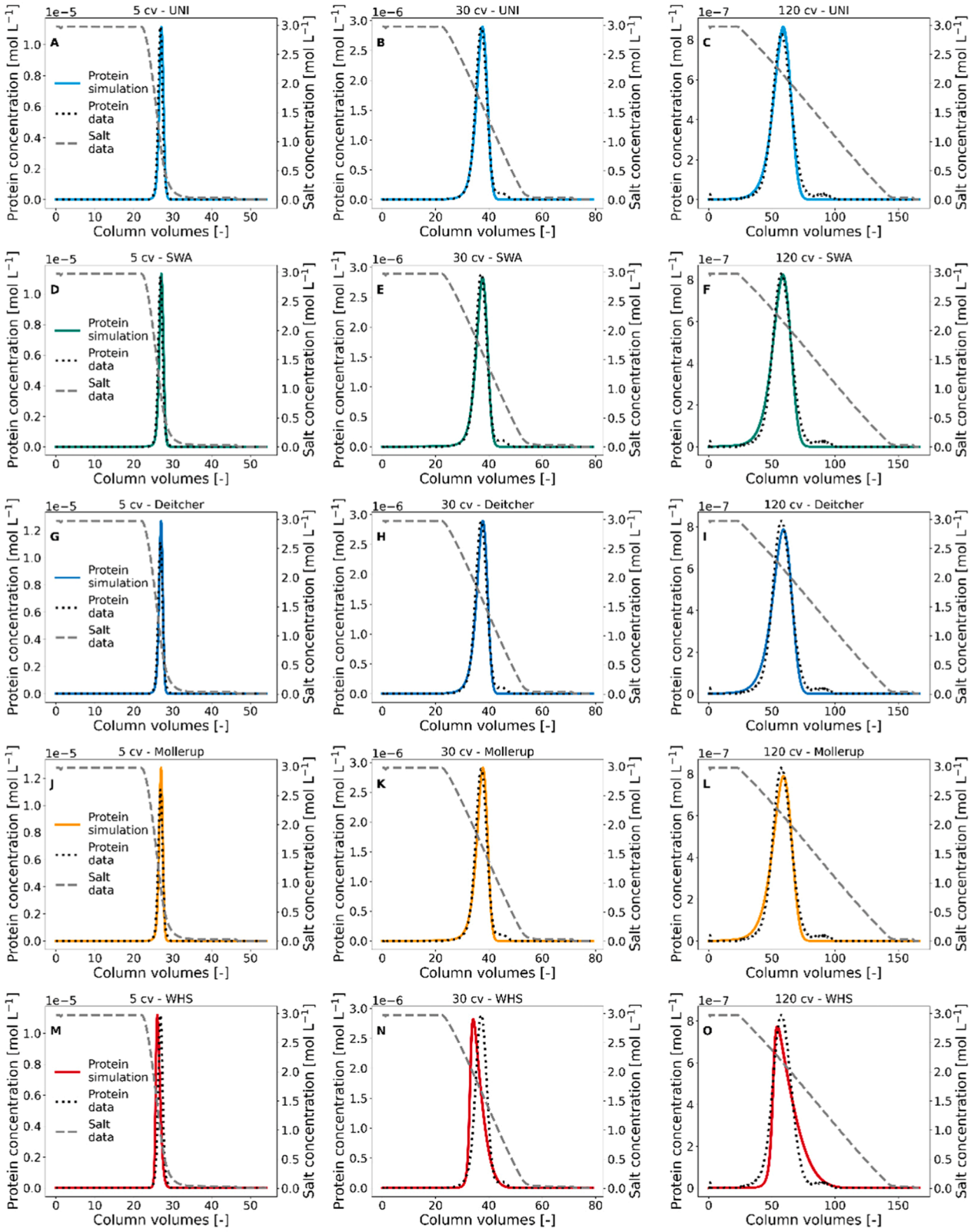

Fig. 6. Isotherm performance for lysozyme on Butyl Sepharose 4 FF at pH 7.0. Comparison of simulated chromatograms based on parameter predictions (from three individual fits) using 5 cv (first column of graphs) 30 cv (second column of graphs) or 120 cv (third column of graphs) and five different isotherms (Unified (UNI) – row 1; Salt-dependent water activity (SWA) – row 2; Deitcher – row 3; Mollerup – row 4; Water on hydrophobic surfaces (WHS) – row 5) (Supplementary Table 3).

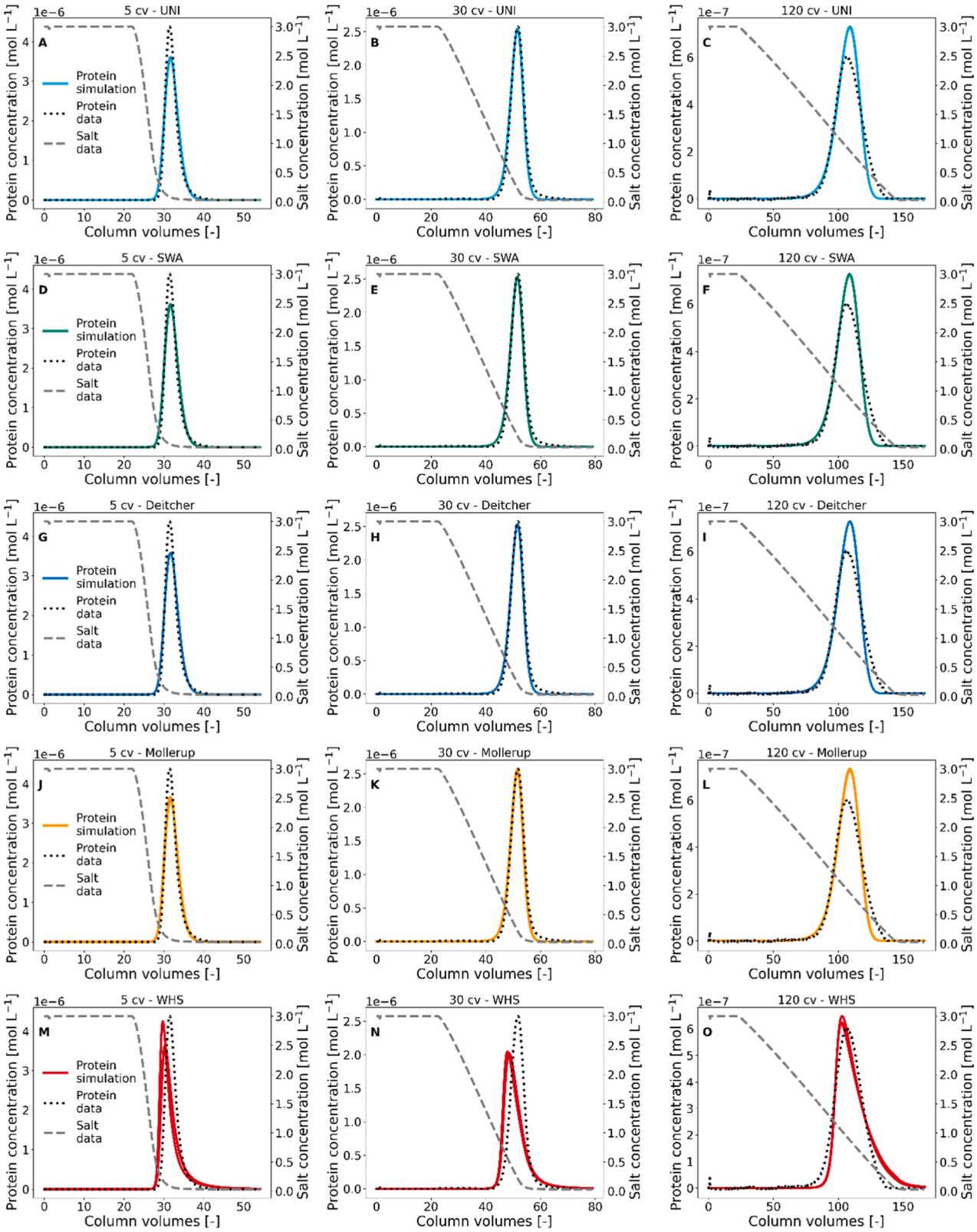

Fig. 7. Isotherm performance for lysozyme on Phenyl Sepharose at pH 7.0. Comparison of simulated chromatograms based on parameter predictions (from three individual fits) using 5 cv (first column of graphs) 30 cv (second column of graphs) or 120 cv (third column of graphs) and five different isotherms (Unified (UNI) – row 1; Salt-dependent water activity (SWA) – row 2; Deitcher – row 3; Mollerup – row 4; Water on hydrophobic surfaces (WHS) – row 5) (Supplementary Table 3).

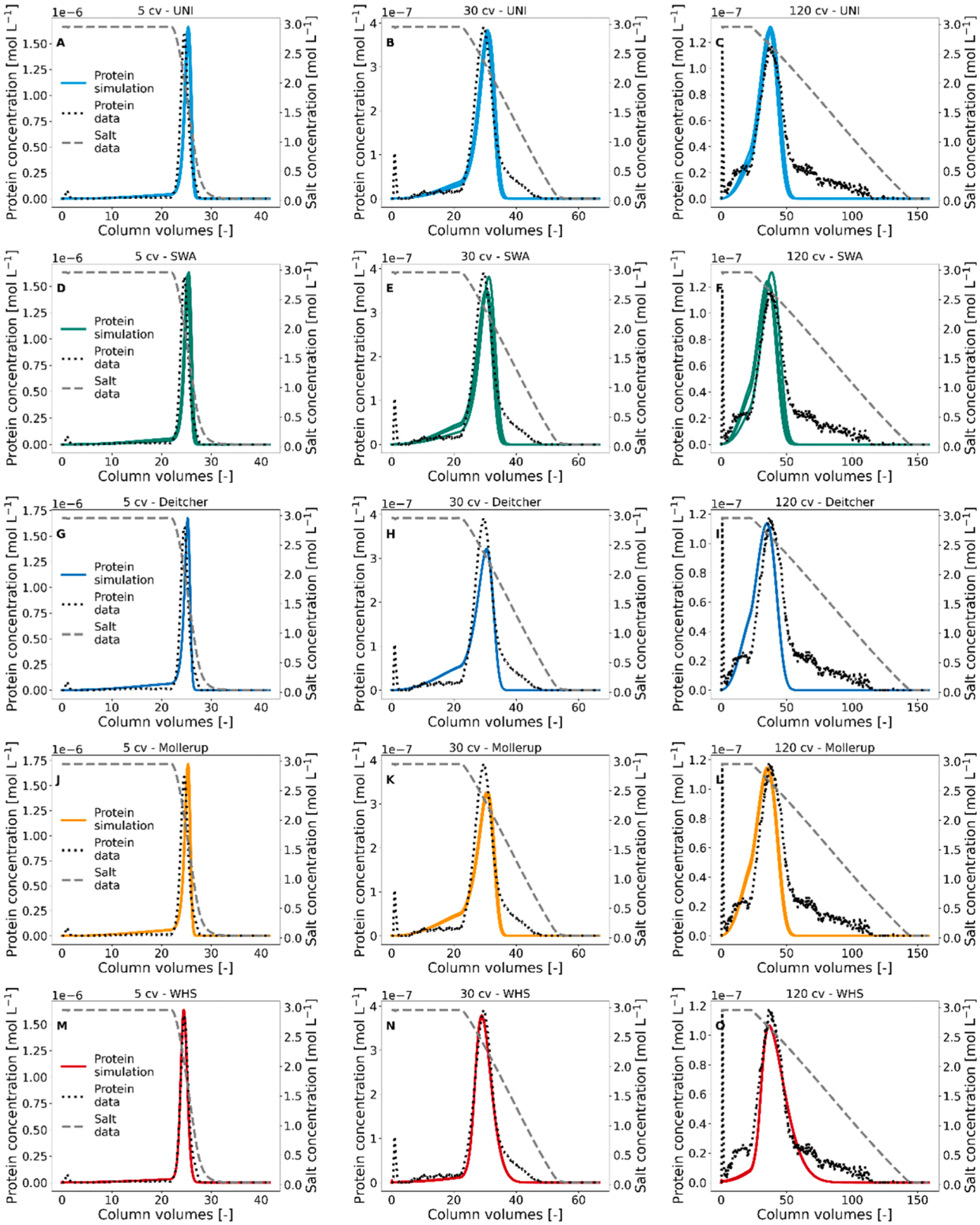

Fig. 8. Isotherm performance for albumin on Butyl-S Sepharose at pH 7.0. Comparison of simulated chromatograms based on parameter predictions (from three individual fits) using 5 cv (first column of graphs) 30 cv (second column of graphs) or 120 cv (third column of graphs) and five different isotherms (Unified (UNI) – row 1; Salt-dependent water activity (SWA) – row 2; Deitcher – row 3; Mollerup – row 4; Water on hydrophobic surfaces (WHS) – row 5) (Supplementary Table 3).

works by introducing a salt-dependent water activity as one of the driving factors of component desorption. The precision of elution profile prediction, measured as the differences in elution peak height, skew and position, improved by an average of 2.8-fold and up to 5.6-fold over three experimental datasets compared to previous isotherms. We have implemented the buffer pH as an additional variable in the isotherm in CADET, facilitating rapid calibration to different experimental settings. Furthermore, when implementing the new isotherm into the CADET modeling suit, we unified it with previous parametrizations to facilitate a fast and easy comparison of different isotherm variants. In the future, expanding the isotherm for additional process parameters such as temperature can hold additional value when implementing HIC for in silico process optimization. However, it will be important to balance the benefits of additional parameters against the risk of overfitting. In this context it is important to note that our new isotherm does not increase the number of fitting parameters but only uses variables that are defined by the experimental conditions, such as salt concentration and activity. In the future, we will verify the performance of the new isotherm using additional proteins, ligands and salt types as well as high loading densities to reflect conditions during preparative protein purification.

Declarations

Ethics approval

Not applicable.

Funding

This work was funded in part by the Fraunhofer-Gesellschaft through grant 125–600,164.

Consent for publication

All authors have seen a draft version of the manuscript and concur with its submission to the journal.

Code availability *(software application or custom code)*

Not applicable.

CRediT authorship contribution statement

Ronald Jäpel: Writing – original draft, Visualization, Software, Methodology, Investigation, Formal analysis, Data curation. **Matthias Knödler:** Data curation. **Eric von Lieres:** Writing – review & editing, Validation, Supervision, Software, Funding acquisition. **Johannes Felix Buyel:** Writing – review & editing, Writing – original draft, Supervision, Software, Resources, Project administration, Methodology, Funding acquisition, Conceptualization.

Declaration of competing interest

The authors declare the following financial interests/personal relationships which may be considered as potential competing interests:

Johannes Felix Buyel reports financial support was provided by Fraunhofer Society for the Advancement of Applied Research. If there are other authors, they declare that they have no known competing financial interests or personal relationships that could have appeared to influence the work reported in this paper.

Acknowledgements

We wish to thank Prof. Dr. Rainer Hahn for constructive discussions.

Supplementary materials

Supplementary material associated with this article can be found, in the online version, at doi:10.1016/j.chroma.2025.466095.

Data availability

Data will be made available on request.

References

[1] I.R.A. Pereira Bresolin, N. Lingg, I.T.L. Bresolin, A. Jungbauer, Hydrophobic interaction chromatography as polishing step enables obtaining ultra-pure recombinant antibodies, J. Biotechnol. 324S (2020) 100020, https://doi.org/10.1016/j.btecx.2020.100020.
[2] C. Stamatis, S. Goldrick, D. Gruber, R. Turner, N.J. Titchener-Hooker, S.S. Farid, High throughput process development workflow with advanced decision-support for antibody purification, J. Chromatogr. A 1596 (2019) 104–116, https://doi.org/10.1016/j.chroma.2019.03.005.
[3] C.R. Bernau, M. Knödler, J. Emonts, R.C. Jäpel, J.F. Buyel, The use of predictive models to develop chromatography-based purification processes, Front. Bioeng. Biotechnol. 10 (2022) 1009102, https://doi.org/10.3389/fbioe.2022.1009102.
[4] K.W. Brhane, S. Qamar, A. Seidel-Morgenstern, Two-dimensional general rate model of liquid chromatography incorporating finite rates of adsorption–Desorption kinetics and core–Shell particles, Ind. Eng. Chem. Res. 58 (2019) 8296–8308, https://doi.org/10.1021/acs.iecr.9b00364.
[5] N. Kaiblinger, R. Hahn, J. Beck, Y. Wang, G. Carta, Direct calculation of the equilibrium composition for multi-component langmuir isotherms in batch adsorption, Adsorption 30 (2023) 51–56, https://doi.org/10.1007/s10450-023-00429-4.
[6] J.M. Mollerup, Applied thermodynamics: a new frontier for biotechnology: a new frontier for biotechnology, Fluid Phase Equilibr 241 (2006) 205–215, https://doi.org/10.1016/j.fluid.2005.12.037.
[7] R.W. Deitcher, J.E. Rome, P.A. Gildea, J.P. O'Connell, E.J. Fernandez, A new thermodynamic model describes the effects of ligand density and type, salt concentration and protein species in hydrophobic interaction chromatography, J. Chromatogr. A 1217 (2010) 199–208, https://doi.org/10.1016/j.chroma.2009.07.068.
[8] G. Wang, T. Hahn, J. Hubbuch, Water on hydrophobic surfaces: mechanistic modeling of hydrophobic interaction chromatography: mechanistic modeling of hydrophobic interaction chromatography, J. Chromatogr. A 1465 (2016) 71–78, https://doi.org/10.1016/j.chroma.2016.07.085.
[9] S. Leweke, E. von Lieres, Chromatography analysis and Design toolkit (CADET), Comput. Chem. Eng. 113 (2018) 274–294, https://doi.org/10.1016/j.compchemeng.2018.02.025.
[10] Han Zhang, Viscosity and density of water + sodium chloride + potassium chloride solutions at 298.15 K, J. Chem. Eng. Data 41 (1996) 516–520, https://doi.org/10.1021/je9501402.
[11] L.J. Partanen, J.I. Partanen, Traceable values for activity and osmotic coefficients in aqueous sodium chloride solutions at temperatures from 273.15 to 373.15 K up to the saturated solutions, J. Chem. Eng. Data 65 (2020) 5226–5239, https://doi.org/10.1021/acs.jced.0c00402.
[12] M. El Guendouzi, A. Benbiyi, Thermodynamic properties of binary aqueous solutions of orthophosphate salts, sodium, potassium and ammonium at T=298.15K, Fluid Phase Equilibr 369 (2014) 68–85, https://doi.org/10.1016/j.fluid.2014.02.019.
[13] B.C.S. To, A.M. Lenhoff, Hydrophobic interaction chromatography of proteins. I. The effects of protein and adsorbent properties on retention and recovery, J. Chromatogr. A 1141 (2007) 191–205, https://doi.org/10.1016/j.chroma.2006.12.020.
[14] X. Geng, L. Guo, J. Chang, Study of the retention mechanism of proteins in hydrophobic interaction chromatography, J. Chromatogr. A 507 (1990) 1–23, https://doi.org/10.1016/S0021-9673(01)84176-5.
[15] W. Blokzijl, J.B.F.N. Engberts, Hydrophobic effects. Opinions and facts, Angew. Chem. Int. Edit. 32 (1993) 1545–1579, https://doi.org/10.1002/anie.199315451.
[16] O.W. Howarth, Reassessment of hydrophobic bonding, J. Chem. Soc., Faraday Trans. 1 71 (1975) 2303, https://doi.org/10.1039/F19757102303.
[17] N.T. Southall, K.A. Dill, A.D.J. Haymet, A view of the hydrophobic effect, J. Phys. Chem. B 106 (2002) 521–533, https://doi.org/10.1021/jp015514e.
[18] F. Rossotti, H. Rossotti, The Determination of Stability Constants: And Other Equilibrium Constants in Solution, McGraw-Hill, 1961.
[19] V.N. Afanasiev, A.N. Ustinov, I.Y. Vashurina, Acoustic study of solvent coordination in the hydration shells of potassium iodide, J. Solution Chem. 35 (2006) 1477–1491, https://doi.org/10.1007/s10953-006-9083-4.
[20] S. Leweke, J. Breuer, J. Schmölder, R. Jäpel, H. Lanzrath, J. Rao, J. Hassan, W. Zhang, A. Berger, W. Heymann, E. von Lieres, CADET-core: version 5.0.0, Zenodo, 2024.
[21] M. Knödler, Modeling of hydrophobic interaction chromatography to optimize the downstream processing of biopharmaceuticals. Master thesis, Aachen, Germany, 2018.
[22] R.A. Robinson, R.H. Stokes, Electrolyte Solutions, Second. Rev, Dover Publications, Mineola, NY, 2002.

[23] P. Virtanen, R. Gommers, T.E. Oliphant, M. Haberland, T. Reddy, D. Cournapeau, E. Burovski, P. Peterson, W. Weckesser, J. Bright, S.J. van der Walt, M. Brett, J. Wilson, K.J. Millman, N. Mayorov, A.R.J. Nelson, E. Jones, R. Kern, E. Larson, C. J. Carey, İ. Polat, Y. Feng, E.W. Moore, J. VanderPlas, D. Laxalde, J. Perktold, R. Cimrman, I. Henriksen, E.A. Quintero, C.R. Harris, A.M. Archibald, A.H. Ribeiro, F. Pedregosa, P. van Mulbregt, SciPy 1.0: fundamental algorithms for scientific computing in Python, Nat. Methods 17 (2020) 261–272, https://doi.org/10.1038/s41592-019-0686-2.

[24] T.R.C. van Assche, G.V. Baron, J.F.M. Denayer, An explicit multicomponent adsorption isotherm model: accounting for the size-effect for components with Langmuir adsorption behavior, Adsorption 24 (2018) 517–530, https://doi.org/10.1007/s10450-018-9962-1.

[25] D.M. Ruthven, Principles of Adsorption and Adsorption Processes, Wiley, New York, 1984.

[26] W. Heymann, J. Glaser, F. Schlegel, W. Johnson, P. Rolandi, E. von Lieres, Advanced score system and automated search strategies for parameter estimation in mechanistic chromatography modeling, J. Chromatogr. A 1661 (2022) 462693, https://doi.org/10.1016/j.chroma.2021.462693.

[27] R. Jäpel, Overcoming hurdles in the development of chromatographic models, 2023.